

Electronic Supporting Information (ESI) for

Heterojunction Photocatalyst Composed of Zinc Rhodium Oxide, Single Crystal-Derived Bismuth Vanadium Oxide, and Silver for Overall Pure-Water Splitting under Visible Light up to 740 nm

Ryoya Kobayashi,^a Toshihiro Takashima,^b Satoshi Tanigawa,^a Shugo Takeuchi,^c Bunsho Ohtani^d and Hiroshi Irie^{*b,d}

^a. *Special Doctoral Program for Green Energy Conversion Science and Technology, Interdisciplinary Graduate School of Medicine and Engineering, University of Yamanashi, 4-3-11 Takeda, Kofu, Yamanashi 400-8511, Japan*

^b. *Clean Energy Research Center, University of Yamanashi, 4-3-11 Takeda, Kofu, Yamanashi 400-8511, Japan*

^c. *Graduate School of Environmental Science, Hokkaido University, Nishi 10, Nishi 5, Sapporo, Hokkaido 060-0810, Japan*

^d. *Institute for Catalysis, Hokkaido University, Nishi 10, Kita 21, Sapporo, Hokkaido 001-0021, Japan*

Contents

ESI. 1 Description of previously developed overall water-splitting photocatalysts.

ESI. 2 Back-reflection Laue pattern of s-Bi₄V₂O₁₁ (Fig. S1).

ESI. 3 Photos of pulverized s-Bi₄V₂O₁₁, as-prepared ZnRh₂O₄, and ZnRh₂O₄/Ag/p-Bi₄V₂O₁₁ after HNO₃ treatment (Fig. S2).

ESI. 4 Comparison of s-Bi₄V₂O₁₁ and p-Bi₄V₂O₁₁ regarding UV-vis and PA spectra, and AQE (Fig. S3).

ESI. 5 Overall pure-water splitting over ZnRh₂O₄/Ag/s-Bi₄V₂O₁₁ irradiated with visible light (>420 nm) (Fig. S4). Comparison of ZnRh₂O₄/Ag/s-Bi₄V₂O₁₁ before and after performing the water-splitting reaction (Figs. S5 and S6).

ESI. 6 O₂ generation rates under different LED light sources, normalized photon numbers, and QE values for overall pure-water splitting (Table S1).

ESI. 7 Energy band diagram and charge transfer process for ZnRh₂O₄/Ag/Bi₄V₂O₁₁ (Scheme S1).

ESI. 1 Description of previously developed overall water-splitting photocatalysts.

Numerous groups have attempted to identify powdered photocatalysts that are able to split water into H_2 and O_2 at a molar ratio of $\sim 2 : 1$ (overall water splitting) under visible-light irradiation for the efficient utilization of sunlight energy. One major approach for visible-light sensitization is to construct a system composed of a single photocatalyst with a controlled electric band structure and a suitable cocatalyst.⁸⁻¹⁶ The most well-known example of such a system is gallium nitride (GaN)–zinc oxide (ZnO) solid solution reported by Domen *et al.*⁸⁻¹¹ More recently, several novel photocatalysts have been developed,¹²⁻¹⁹ including nanocrystalline CoO, which exhibits visible-light sensitivity even in the absence of a cocatalyst.¹⁷ Pan *et al.*¹⁸ also developed a complex photocatalyst, titanium-and-silicon amorphous oxyhydroxide ($MO_{2-m}(OH)_{2m} \cdot xH_2O$)-coated Rh–Cr oxide ($RhCrO_y$)-loaded lanthanum–magnesium–tantalum oxynitride ($LaMg_xTa_{1-x}O_{1+3x}N_{2-3x}$) solid solution, which has an E_g of 2.03 eV and is reported to function at wavelengths up to 600 nm. Liu *et al.*¹⁹ synthesized a carbon nanodot (CDot)–carbon nitride (C_3N_4) nanocomposite as a metal-free photocatalyst and demonstrated that this material is capable of overall water splitting when irradiated with visible light with a wavelength of 630 ± 20 nm, which is the longest reported wavelength for overall water splitting using this approach. Another approach for visible-light sensitization is the construction of systems composed of two photocatalysts that are both sensitive to visible light, called “Z-scheme” systems. Previous studies on Z-scheme photocatalysts are described in the main text.

ESI. 2 Back-reflection Laue pattern of $s-Bi_4V_2O_{11}$ (Fig. S1).

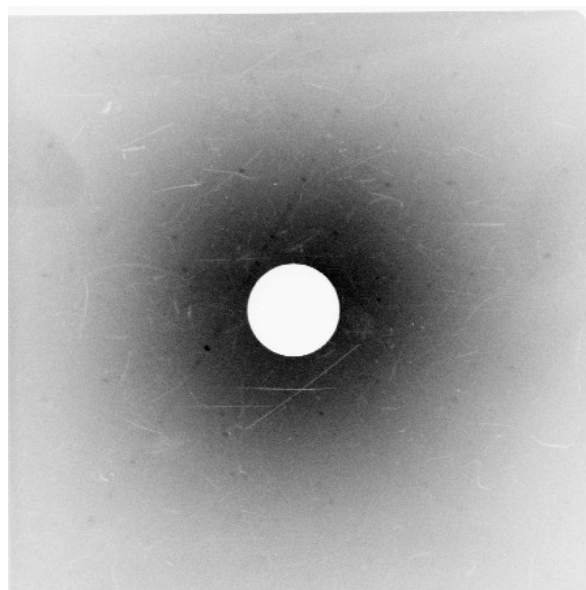


Fig. S1 Back-reflection Laue pattern taken from the normal to plate surface of a single $Bi_4V_2O_{11}$ crystal. Black spots correspond to the Laue pattern. The visible white markings were due to flaws in the film.

ESI. 3 Photos of pulverized $s\text{-Bi}_4\text{V}_2\text{O}_{11}$, as-prepared ZnRh_2O_4 , and $\text{ZnRh}_2\text{O}_4/\text{Ag}/p\text{-Bi}_4\text{V}_2\text{O}_{11}$ after HNO_3 treatment (Fig. S2).



Fig. S2 Photos showing pulverized $s\text{-Bi}_4\text{V}_2\text{O}_{11}$ (a), as-prepared ZnRh_2O_4 (b), and $\text{ZnRh}_2\text{O}_4/\text{Ag}/p\text{-Bi}_4\text{V}_2\text{O}_{11}$ after HNO_3 treatment (c).

ESI. 4 Comparison of $s\text{-Bi}_4\text{V}_2\text{O}_{11}$ and $p\text{-Bi}_4\text{V}_2\text{O}_{11}$ regarding UV-vis and PA spectra, and AQE (Fig. S3).

The PA spectrum intensity of $s\text{-Bi}_4\text{V}_2\text{O}_{11}$ was larger than that of $p\text{-Bi}_4\text{V}_2\text{O}_{11}$, corresponding to their UV-visible absorption capability. The reasons for the observation are still unknown; however, the higher true absorption capability of $s\text{-Bi}_4\text{V}_2\text{O}_{11}$ would be one reason for the enhanced AQE, as well as the higher crystallinity and anisotropy.

Similar to the case of $s\text{-Bi}_4\text{V}_2\text{O}_{11}$, the AQE values for O_2 evolution of $p\text{-Bi}_4\text{V}_2\text{O}_{11}$ coincided with the PA absorption spectrum, but not with the UV-vis absorption spectrum.

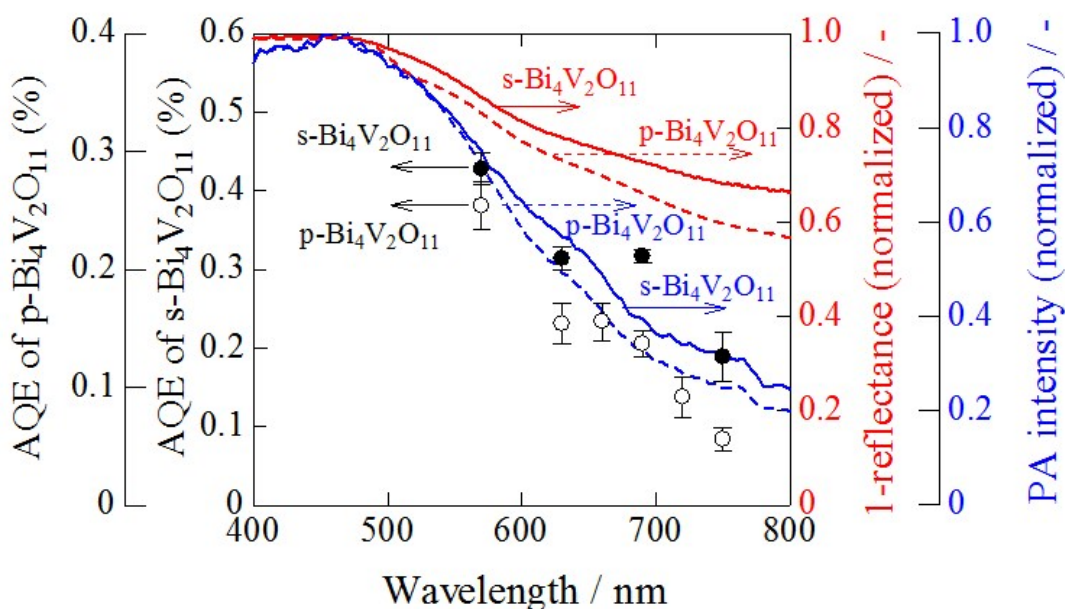


Fig. S3 Action spectra for O_2 evolution by the half reaction of water over $s\text{-Bi}_4\text{V}_2\text{O}_{11}$ (solid circles) and $p\text{-Bi}_4\text{V}_2\text{O}_{11}$ (open circles) in the presence of Ce^{4+} . The data are the same as those in Fig. 7. The normalized UV-visible absorption spectra of $s\text{-Bi}_4\text{V}_2\text{O}_{11}$ (red solid line) and $p\text{-Bi}_4\text{V}_2\text{O}_{11}$ (red broken line), and the normalized PA spectra of $p\text{-Bi}_4\text{V}_2\text{O}_{11}$ (blue solid line) and $s\text{-Bi}_4\text{V}_2\text{O}_{11}$ (blue broken line) are also shown.

ESI. 5 Overall pure-water splitting over $\text{ZnRh}_2\text{O}_4/\text{Ag}/\text{s-Bi}_4\text{V}_2\text{O}_{11}$ irradiated with visible light (>420 nm) (Fig. S4). Comparison of $\text{ZnRh}_2\text{O}_4/\text{Ag}/\text{s-Bi}_4\text{V}_2\text{O}_{11}$ before and after performing the water-splitting reaction (Figs. S5 and S6).

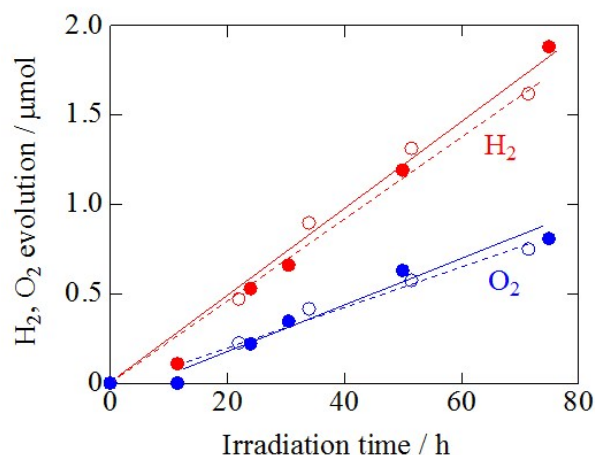


Fig. S4 Time courses of photocatalytic evolution of H_2 and O_2 from pure water over $\text{ZnRh}_2\text{O}_4/\text{Ag}/\text{s-Bi}_4\text{V}_2\text{O}_{11}$ irradiated with visible light (>420 nm).

We measured the XRD pattern of $\text{ZnRh}_2\text{O}_4/\text{Ag}/\text{s-Bi}_4\text{V}_2\text{O}_{11}$ powder after performing the water-splitting reaction under the conditions used in Fig. S4. Notably, however, the XRD pattern did not change after the reaction, as shown in Fig. S5. Also note that the XRD pattern in Fig. S5 denoted as “Before water splitting” is the same as that presented in Fig. 3.

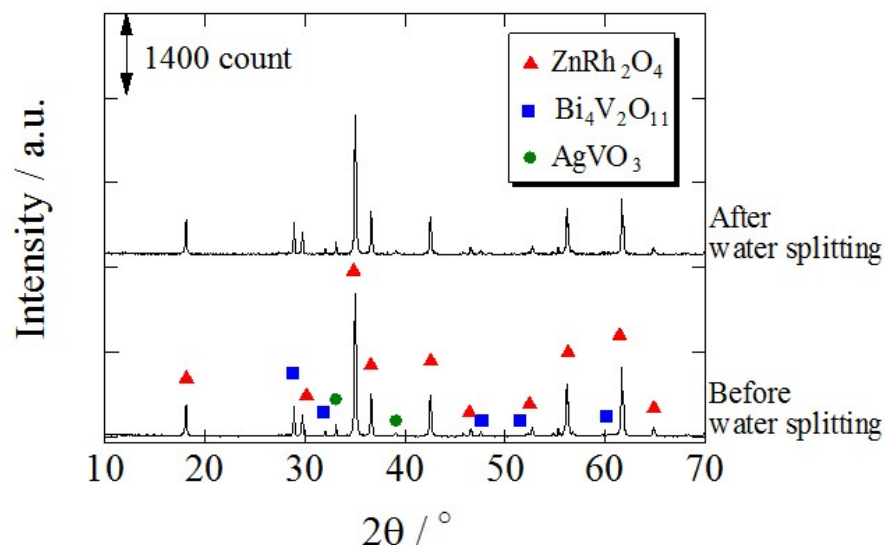


Fig. S5 XRD patterns of HNO_3 -treated $\text{ZnRh}_2\text{O}_4/\text{Ag}/\text{s-Bi}_4\text{V}_2\text{O}_{11}$ before and after performing the water-splitting reaction.

STEM imaging and EDS-based elemental mapping of $\text{ZnRh}_2\text{O}_4/\text{Ag}/\text{Bi}_4\text{V}_2\text{O}_{11}$ after the water-splitting reaction (Fig. S4) were also performed (Figs. S6a–S6e). In the STEM image of $\text{ZnRh}_2\text{O}_4/\text{Ag}/\text{Bi}_4\text{V}_2\text{O}_{11}$ before the water-splitting reaction (Figs. 6a and 6b), *s*- $\text{Bi}_4\text{V}_2\text{O}_{11}$ and ZnRh_2O_4 particles were clearly distinguishable (Figs. S6a and S6b) based on size. Although the number of ZnRh_2O_4 particles that were not attached to the $\text{Bi}_4\text{V}_2\text{O}_{11}$ surface before the water-splitting reaction appeared to have decreased after the reaction, Ag was distributed (Fig. S6e) between the Bi (Fig. S6c) and Rh sites (Fig. S6d), as was observed in Figs. 6c–6e. $\text{ZnRh}_2\text{O}_4/\text{Ag}/\text{Bi}_4\text{V}_2\text{O}_{11}$ did not appear to have changed even after performing the water-splitting reaction, and Ag was detected between the ZnRh_2O_4 and $\text{Bi}_4\text{V}_2\text{O}_{11}$ particles.

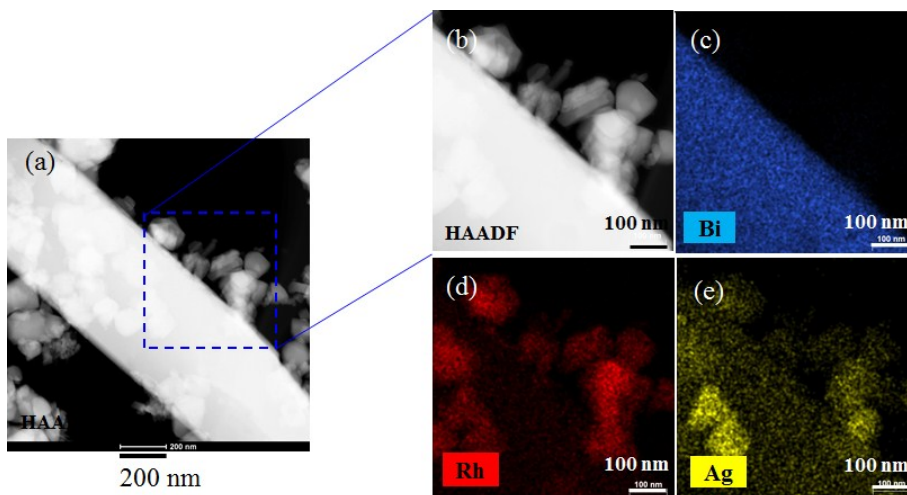


Fig. S6 STEM images of $\text{ZnRh}_2\text{O}_4/\text{Ag}/\text{s-Bi}_4\text{V}_2\text{O}_{11}$ after performing the water-splitting reaction under the conditions in Fig. S4. STEM image (a), its enlargement (b), and EDS element maps (c–e), in which the blue (c), red (d), and yellow (e) colors correspond to Bi, Rh, and Ag, respectively.

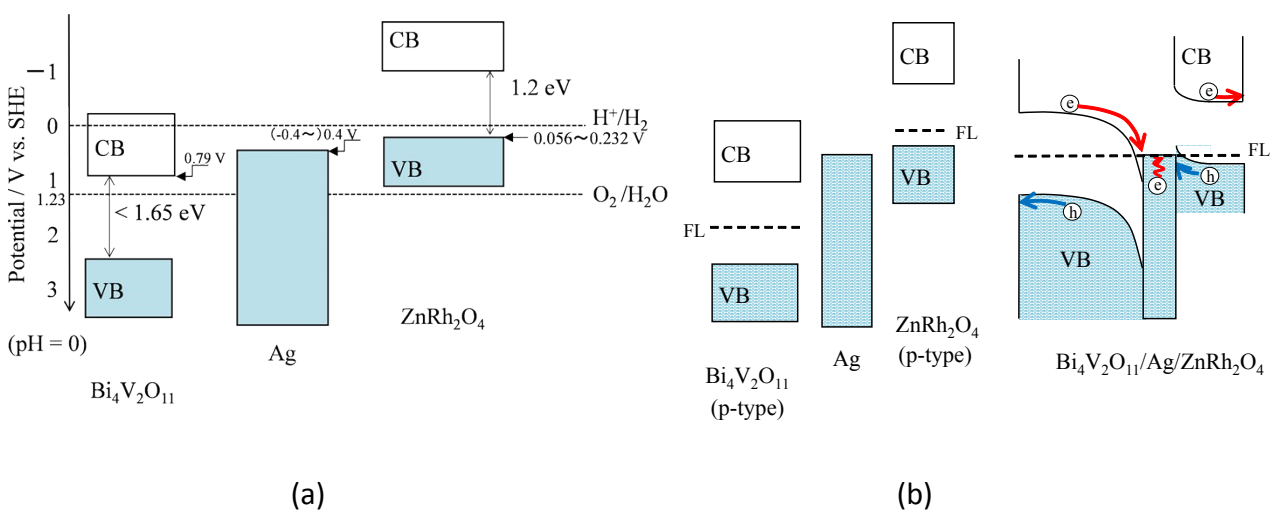
ESI. 6 O₂ generation rates under different LED light sources, normalized photon numbers, and QE values for overall pure-water splitting (Table S1).

Table S1 O₂ generation rates, normalized photon numbers, and QE values for overall pure-water splitting over ZnRh₂O₄/Ag/s-Bi₄V₂O₁₁.

Light source	Light intensity / mW cm ⁻²	O ₂ generation rate / μmol h ⁻¹	AQE (%)
545 nm LED	1.54	1.31×10 ⁻²	3.45×10 ⁻²
610 nm LED	1.40	8.97×10 ⁻³	2.33×10 ⁻²
700 nm LED	4.00	1.36×10 ⁻²	1.07×10 ⁻²
740 nm LED	3.06	3.32×10 ⁻³	3.25×10 ⁻³

ESI. 7 Energy band diagram and charge transfer process for $\text{ZnRh}_2\text{O}_4/\text{Ag}/\text{Bi}_4\text{V}_2\text{O}_{11}$ (Scheme S1).

The band edge positions of ZnRh_2O_4 , Ag, and $\text{Bi}_4\text{V}_2\text{O}_{11}$ are described in Scheme S1a and were determined as described in our previous paper.²⁷ The band alignments of ZnRh_2O_4 , Ag, and $\text{Bi}_4\text{V}_2\text{O}_{11}$ before and after the mixing and calcination of Ag and ZnRh_2O_4 , and Ag and $\text{Bi}_4\text{V}_2\text{O}_{11}$ are shown in Scheme S1b. It should be noted that the uncertainty in the band edge positions for ZnRh_2O_4 , Ag, and $\text{Bi}_4\text{V}_2\text{O}_{11}$ would correspond to a few tenths of an eV. In addition, various values for the work function of Ag have been reported depending on the surface states and measuring technique used. Further, although we could not determine the Fermi potentials of ZnRh_2O_4 and $\text{Bi}_4\text{V}_2\text{O}_{11}$, photogenerated holes in the VB of $\text{Bi}_4\text{V}_2\text{O}_{11}$ and photoexcited electrons in the CB of ZnRh_2O_4 evolved O_2 and H_2 , respectively, from water. Scheme S1b was revised to show that holes in the VB of $\text{Bi}_4\text{V}_2\text{O}_{11}$ and electrons in the CB of ZnRh_2O_4 have thermodynamic potentials that allow for O_2 and H_2 evolution, respectively. Thus, the illustration in Scheme 1 was revised from our previous paper.²⁷



Scheme S1 Band edge positions of ZnRh_2O_4 , Ag and $\text{Bi}_4\text{V}_2\text{O}_{11}$ (a) and their band alignments before and after the mixing and calcination of Ag and ZnRh_2O_4 , and Ag and $\text{Bi}_4\text{V}_2\text{O}_{11}$ (b). The charge transfer processes are also shown.